Biochimica et Biophysica Acta 1827 (2013) 10–18

Contents lists available at SciVerse ScienceDirect

Biochimica et Biophysica Acta

journal homepage: www.elsevier.com/locate/bbabio

Variations in the first steps of photosynthesis for the diatom *Cyclotella meneghiniana* grown under different light conditions

V.U. Chukhutsina [a], C. Büchel [c], H. van Amerongen [a,b,*]

[a] *Laboratory of Biophysics, Wageningen University, Wageningen, The Netherlands*
[b] *MicroSpectroscopy Centre, Wageningen University, Wageningen, The Netherlands*
[c] *Institute for Molecular Bio Sciences, Johann Wolfgang Goethe-University, Frankfurt am Main, Germany*

ARTICLE INFO

Article history:
Received 25 June 2012
Received in revised form 19 September 2012
Accepted 25 September 2012
Available online 1 October 2012

Keywords:
Time-resolved fluorescence
Fucoxanthin-chlorophyll protein
Light harvesting
Photosystem I
Photosystem II
Excitation energy transfer

ABSTRACT

In this work we have applied picosecond and steady-state fluorescence measurements to study excitation energy transfer and trapping in intact *Cyclotella meneghiniana* diatom cells grown at different light intensities. Different excitation and detection wavelengths were used to discriminate between Photosystem I and II (PSI and PSII) kinetics and to study excitation energy transfer from the outer antenna to the core of PSI and PSII. It is found that the light-harvesting fucoxanthin chlorophyll proteins (FCPs) transfer their excitation energy predominantly to PSII. It is also observed that the PSII antenna is slightly richer in red-absorbing fucoxanthin than the FCPs associated with PSI. The average excitation trapping time in PSI is around 75 ps whereas this time is around 450 ps for PSII in cells grown in 20 μmol of photons per m^2 per s. The latter time decreases to 425 ps for 50 μmol of photons and 360 ps for 140 μmol of photons. It is concluded that cells grown under higher photon flux densities have a smaller antenna size than the ones grown in low light. At the same time, the increase of growth light intensity leads to a decrease of the relative amount of PSI. This effect is accompanied by a substantial increase in the amount of chlorophyll *a* that is not active in excitation energy transfer and most probably attached to inactivated/disassembled PSII units.

1. Introduction

Diatoms, unicellular eukaryotes, capable of performing oxygenic photosynthesis, are ecologically important in both fresh water and marine ecosystems with their key role in the biochemical cycles of carbon, nitrogen, phosphorus and silica [1]. In contrast to higher plants, their thylakoid membranes are not segregated into stromal and granal regions. However, like in plants their antenna complexes, the so-called fucoxanthin-chlorophyll *a*/*c* proteins (FCPs), are also membrane-intrinsic (for reviews, see [2], [3]).

Since recently various research groups have studied the photosynthesis apparatus of diatoms. In many cases they perform *in vitro* studies on the FCPs (see e.g. [4–7]), but also research has been performed on intact cells [8–10].

Although the antenna complexes in this alga belong to the light-harvesting chlorophyll (Chl) protein (LHC) superfamily [11], their pigment content differs from that of LHCII in higher plants. FCPs do not possess Chl *b* but use Chl *c* as an accessory pigment, and they contain fucoxanthin (fx) as the major light-harvesting xanthophyll. Also the chlorophyll:carotenoid stochiometry of the light-harvesting antennae of diatoms differs from that of higher plants, with the Chl *a*: carotenoid ratio being 1:1 [4,6,12], much lower than for plants where it is around 3 (see e.g. [12]).

Two major fractions of FCPs were observed in *Cyclotella meneghiniana*, differing both in their polypeptide composition and oligomeric state: one fraction contains trimeric FCPa, consisting of mainly 18 kDa proteins and only small amounts of 19 kDa subunits whereas FCPb in another fraction is associated into higher oligomeric states and contains only 19 kDa polypeptides [5,13]. In *C. meneghiniana* FCPs are mainly found in the trimeric FCPa state, irrespective of the growth light regime [5].

So far not many studies have addressed the processes of excitation energy transfer and charge separation in diatoms. The first femtosecond absorption studies of FCPs showed that energy transfer from Chl *c* to Chl *a* occurs on a time scale of ~100 fs with nearly 100% efficiency. Target analysis on isolated FCPs also revealed that the EET efficiency from fx, which was excited at 530 nm, to Chl *a* reaches around 80% [4], while FCPa samples show a somewhat higher energy transfer efficiency than oligomeric FCPb forms, irrespective of the excitation wavelength [6]. Some structural differences between the complexes

Abbreviations: Chl, chlorophyll; DAS, decay-associated spectra; ddx, diadinoxanthin; dtx, diatoxanthin; EET, excited state absorption; FCP, fucoxanthin-chlorophyll $a/c_{1,2}$ protein; fx, fucoxanthin; fx_{blue}, blue-absorbing fucoxanthin; fx_{red}, red-absorbing fucoxanthin; FWHM, the full-width at half-maximum; ICT, intramolecular charge transfer; LHC, light-harvesting chlorophyll protein; NPQ, nonphotochemical quenching; OD, optical density; PS, photosystem; PSU, photosynthetic unit; RC, reaction center; TCSPC, Time-correlated single photon counting

* Corresponding author at: Laboratory of Biophysics, Wageningen University, Wageningen, The Netherlands. Fax: +31 317 482725.
E-mail address: herbert.vanamerongen@wur.nl (H. van Amerongen).

0005-2728/$ – see front matter © 2012 Elsevier B.V. All rights reserved.
http://dx.doi.org/10.1016/j.bbabio.2012.09.015

were observed as well: trimeric FCP binds relatively more fx than higher oligomers [5–7]. Stark and resonance Raman spectroscopy data were the first to show the existence of different fx forms in FCPs [14,15]. From the excitation and absorption spectra of different FCPs populations it can be observed that oligomeric FCPb shows slightly less absorption around 490 nm and increased values around 540 nm as compared to FCPa trimers [5–7], implying that trimers might bind more blue-shifted fx as compared to FCPb.

For a long time it was believed that the two types of FCP are associated with both photosystem (PS) I and PSII but this topic is still under debate [16–18]. Veith et al. for instance found that the Fcp5 polypeptide that is part of FCPb, is loosely bound to PSI complexes [5,13,19]. On the other hand, Szabo et al. provided experimental evidence that inside intact diatom cells fx_{red} (presumably FCPb, see above) binds to PSII in a slightly greater amount than to PSI [9].

Recently, the first ps fluorescence study of intact diatoms was performed [8]. The fluorescence kinetics of two diatom species were analyzed with the use of global target analysis. Six components were used to describe the kinetics of both PSI and PSII in the open state (three for PSI and three for PSII). The average lifetime of the overall PSI kinetics was found to be ~51 ps for *C. meneghiniana* and 100 ps for *P. tricornutum*, while the total contribution of PSII was described by an average lifetime of ~395 ps for *C. meneghiniana* and ~432 ps for *P. tricornutum*. A detailed model was proposed as well to describe the occurrence of nonphotochemical quenching (NPQ) at two independent quenching sites. One was thought to be located in FCP that detaches from PSII during NPQ while the second one is located in the PSII-associated antenna.

The investigation of the long-time response of diatoms to different light conditions is another topic of growing scientific interest. Diatoms are known to have interesting acclimation mechanisms, responding to alterations in growth irradiance. One of them includes the adjustment of the ratio between PSII and PSI. The PSII:PSI ratio increases when the light intensity decreases in *Thalassiosira weissflogii*, a species closely related to *C. meneghiniana*, (LL — 2.2:1, HL — 4.4:1) [20] and in *Skeletonema costatum* from LL 0.4 to HL 1 [21] (Falkowski et al 1981).On the other hand, Smith and Melis found exactly the opposite in *Cylindrotheca fusiformis* (HL — 1.3:1; LL —3.9:1)[22].

A change in the photon flux density also leads to a change in the size of the photosynthetic units (PSU). Gallagher et al. were the first to report a decrease in size of PSI and PSII units in diatom species under high-light conditions [23]. It was concluded that the amount of FCPb is not highly affected by the differences in light intensity but that the amount of FCPa decreases in high-light conditions [5].

In the present work we have studied *C. meneghiniana* with picosecond fluorescence spectroscopy using different excitation and detection wavelengths, linking the resolved spectroscopic features to the various processes taking place, with special attention for the response of the diatoms to different light conditions. A new method is introduced to separate the PSI and PSII excitation spectra of diatoms *in vivo* and it is found that the light-harvesting systems of PSI and PSII have different spectroscopic properties in agreement with recent experimental data [9].

2. Materials and methods

2.1. Cell culture

The diatom *C. meneghiniana* (Culture Collection Göttingen, strain 1020-1a) was grown in batch cultures at 18 °C with constant shaking at 120 rpm in low light (LL, 20 μmol photons m^{-2} s^{-1}), medium light (ML, 50 μmol photons m^{-2} s^{-1}) and high light (HL, 140 μmol photons m^{-2} s^{-1}) in the silica-enriched ASP medium according to [24]. A 16 h light: 8 h dark cycle was used in all cases.

Cells were adapted to these light conditions for months, and they were always harvested in the logarithmic growth phase.

2.2. Steady-state fluorescence measurements

2.2.1. Steady-state emission spectra

Steady-state fluorescence spectra were recorded with a Jobin Yvon Fluorolog FL3A22 spectrofluorimeter at 77 K and corrected for wavelength-dependent sensitivity of the detection and fluctuations in the lamp output. The samples were diluted with 60% glycerol (v/v). Two excitation wavelengths were used: 400 nm and 535 nm; a bandwidth of 3 nm was used both for the excitation and the emission branch. Fluorescence emission spectra were recorded using a step size of 0.5 nm.

To minimize re-absorption the samples were adjusted to an absorbance of 0.04/cm in the Q_y band of Chl *a*.

Different wavelengths were used in order to modulate the relative amount of excitations in the core and the outer antenna complexes by using either 400 nm (mainly Chl *a*) and 535 nm (fx) as excitation wavelength. It was shown that Chl *a* dominates the absorption intensity of isolated FCPs in the 400–415 nm region (Chl *a* ~56%, Chl *c* ~36%) [7,14,15]. In case of whole cells, Chl *a* excitation at 400 nm is even more selective because the pigment concentration of Chl *a*, being the major pigment of PSI and PSII cores, rises by ~10% in intact cells (from 40% to 50%), while the Chl *c* concentration decreases from 10% to 5% [25]. The second wavelength (535 nm) was chosen for fx excitation. This antenna-specific carotenoid is responsible for 90% of the absorption for isolated FCPs at this wavelength. This value will not change much in the case of whole cells because both Chl *a*/*c* and Ddx hardly absorb at 535 nm [7,14,15].

2.2.2. Steady-state excitation spectra

For steady-state fluorescence excitation spectra the same Jobin Yvon Fluorolog FL3A22 spectrofluorimeter was used. The fluorescence excitation spectra were recorded between 420 and 650 nm with excitation and emission bandwidths of 2 and 10 nm, respectively. The emission was collected at 680 and 690 nm. An integration time of 0.4 s was used to reduce the noise level. Each spectrum was measured 20 times in a run and then averaged. The sample was measured in two states: an "open" state and a "closed" state. For keeping reaction centers (RCs) open ("open" state), the cells were dark-adapted for 5 min and then kept at 287 K in a flow cuvette and a sample reservoir (5 ml). The sample was flowing from the reservoir to the cuvette and back in darkness, with a flow speed of ~2.5 ml/s. To (partly) close the RCs ("closed" state), 100 μM DCMU was added to the sample and it was preilluminated with relatively strong light (~100 μmol photons m^{-2} s^{-1}). After measuring for 10 min the sample was refreshed. The experiment was repeated two times on cells from different generations.

2.3. Time-resolved fluorescence measurements

2.3.1. Time-correlated single photon counting

Time-correlated single photon counting (TCSPC) measurements were performed at magic angle (54.7°) polarization as described previously [26]. High detection sensitivity and time accuracy are the main advantages of this setup.

In brief, excitation was carried out by ~0.2 ps vertically polarized excitation pulses at a repetition rate of 3.8 MHz. The excitation wavelength was either 400 nm or 535 nm. The sample was kept at 287 K in a flow cuvette and a sample reservoir (5 ml). It was flowing from the reservoir to the cuvette and back, with a speed of ~2.5 ml/s. The optical path length of the cuvette was 3 mm. For each measurement the *C. meneghiniana* sample was diluted to an optical density (OD) of 0.06 per cm at the excitation wavelength (for 400 nm:$OD_{680} \approx 0.04$, for 535 nm: $OD_{680} \approx 0.08$). The size of the excitation spot was 2 mm. In combination with the low laser power (0.5–4 μW), this guaranteed that nearly 100% of the RCs stayed open and a significant buildup of triplet states was avoided (see Supplementary material). Moreover, the 8 ns time window used for the TCSPC measurements makes it possible

to determine "long-lifetime" components that are hard to estimate with alternative techniques. For each run of measurements the following interference filters were used for detection: 671, 679, 693, 701, 712, and 724 nm (15 nm bandwidth) (Balzers, Liechtenstein model B40). The final experiment of a measuring series was always a repetition of the first experiment. The resulting decay curves were indistinguishable (Fig. S2 A in Supplementary material).

Each experiment was repeated 3–5 times for different generations of the cell culture. The decay curves measured for different generations grown under the same light intensities were found to be very reproducible (Fig. S2 B in Supplementary material).

The full-width at half-maximum (FWHM) of the system response function was 35 ps when a resolution of 2 ps per channel was used, as obtained with the 6 ps decay of pinacyanol iodide in methanol [27]. Data analysis was performed using a home-built computer program [28,29]. The data were fitted to multi-exponential decay functions with amplitudes α_i and fluorescence decay times τ_i. For the global analysis the decay lifetimes were forced to be equal for each run of measurements on a sample at a certain excitation wavelength but the amplitudes were allowed to differ. The fit quality was judged from the Poissonian maximum likelihood estimator, the residuals, and the autocorrelation of the residuals [16].

The amplitude-weighted average lifetime was calculated via

$$\tau_{avg} = \sum_{i=1}^{n} \alpha_i * \tau_i \quad (1)$$

where $\sum_{i=1}^{n} a_i = 1$ and τ_i is the lifetime of the i-th component.

2.3.2. Measurements using streak-camera setup

The streak camera allows simultaneous recording of the fluorescence intensity as a function of time and wavelength. This means the output provides entire spectra with a high spectral (few nm) and temporal (~5 ps) resolution. For the fluorescence measurements on the streak-camera setup the sample was diluted to an optical density of 0.09/cm at the excitation wavelength (for 400 nm: $OD_{680} \approx 0.06$, for 535 nm: $OD_{680} \approx 0.13$) and a cuvette with 1 mm optical path was used. Time-resolved emission spectra were recorded using a synchroscan streak-camera system as described in [27,30,31]. Before analysis the images were corrected for the background signal and detector sensitivity and sliced up into traces of 5 nm. An average of 100 images, all measured for 10 s, was used. Each sample was measured with two time windows: 800 ps and 2000 ps. The laser power was typically 15 μW for the 2 ns time window measurements and 35 μW for the 800 ps time window. The spot size was 100 μm while the repetition rate of excitation pulses was 250 kHz. The sample was constantly flowing with a speed of 2.5 ml/s as described in the subsection about time-correlated single photon counting setup (see above).

The streak images were analyzed using the TIMP package for R language [32] and Glotaran, a graphical user interface for the R-package TIMP [33]. A Gaussian-shaped instrument response function was used for the analysis and its width was a free fitting parameter. Typical fwhm values obtained from the fitting procedure are: ~10 ps for the 800 ps time window, ~23 ps for the 2 ns time window. The synchroscan period (13.17 ns) results in the back and forth sweeping of long-lived components and leads to some signal before time zero in the streak-camera images [34]. This is used for long-lived-component estimation. The fit quality was judged by singular value decomposition of the residuals matrix [32].

All experiments were performed at room temperature (293 K).

2.4. Extraction of PSII and PSI excitation spectra from steady-state measurements

When it is assumed that the amount of detached antenna complexes is negligible then the fluorescence excitation spectrum $F(\lambda_{exc})$ is a linear combination of the excitation spectra $PSI(\lambda_{exc})$ and $PSII(\lambda_{exc})$ of PSI and PSII, respectively:

$$F^{open}(\lambda_{exc}) = q_1 * PSI(\lambda_{exc}) + {q_2}^{open} * PSII(\lambda_{exc}) \quad (2)$$

The subscript "open" indicates that the PSII RCs are open in this case. When the RCs are partly closed the excitation spectrum becomes:

$$F^{closed}(\lambda_{exc}) = q_1 * PSI(\lambda_{exc}) + {q_2}^{closed} * PSII(\lambda_{exc}) \quad (3)$$

and due to the increased fluorescence lifetime of closed PSII, its contribution q_2^{closed} to the fluorescence excitation spectrum increases substantially. Note that the contribution of PSI is independent of the fact whether its RC is open or closed [35]. Therefore, by taking the difference between these two excitation spectra (2) and (3), one obtains the PSII excitation spectrum multiplied by a constant, i.e.:

$$PSII(\lambda_{exc}) = \left(1/\left({q_2}^{closed} - {q_2}^{open}\right)\right) * \left(F^{closed}(\lambda_{exc}) - F^{open}(\lambda_{exc})\right) \quad (4)$$

The excitation spectrum of PSI can now be obtained by subtracting $PSII(\lambda_{exc})$ from $F^{open}(\lambda_{exc})$ after proper scaling of the spectra to each other. We measured the excitation spectra by detecting at 679 nm at which wavelength also time-resolved measurements were performed with excitation wavelength 400 nm. The relative or fractional contribution of PSII to the fluorescence can then be estimated according to:

$${E_{PSII}}^{ex/det} = \alpha_2 * \tau_2 / (\alpha_1 * \tau_1 + \alpha_2 * \tau_2) \quad (5)$$

where α_1, α_2 are the amplitudes and τ_1 and τ_2 are the (average) fluorescence lifetimes of PSI and PSII, respectively. In other words

$$PSII(400\,\mathrm{nm}) = {E_{PSII}}^{ex/\mathrm{det}} * F^{open}(400\,\mathrm{nm}) \quad (6)$$

and this allows proper scaling of the excitation spectra at 400 nm, which of course also fixes the relative values at all other excitation wavelengths. Therefore, the PSI excitation spectrum can be estimated according to:

$$PSI(\lambda_{exc}) = F^{open}(\lambda_{exc}) - k^{PSII(400\,\mathrm{nm})} * PSII(\lambda_{exc}) \quad (7)$$

where $k^{PSII(400nm)}$ is a scaling parameter obtained according to (6) and $PSII(\lambda_{exc})$ is the PSII excitation spectrum from Eq. (4).

The procedure was also performed at detection wavelength 693 nm in order to check the consistency of the outcome.

3. Results

3.1. Picosecond kinetics and steady-state fluorescence of C. menegheniana LL cells

Both photosystems in diatoms are composed of a core with FCPs attached to them. It is not possible to excite the cores entirely selectively, because of the strong spectral overlap of outer antenna and core but here we used two excitation wavelengths: 400 nm (the major contribution of Chl *a* absorption) and 535 nm (fx absorption) to modulate the relative amount of excitations in the outer antenna complexes. In this way the corresponding variation in fluorescence kinetics makes it possible to study EET from FCPs to both photosystems *in vivo*.

Global analysis of streak-camera data, obtained after 400 nm and 535 nm excitation leads to the decay-associated spectra (DAS) in Fig. 1. Three components are sufficient to fit the data in both cases. The quality of the fits was judged by left and right vectors of singular

value decomposition of the residuals matrix (for more information about parameter estimation in Glotaran read [32]; [33]).

Upon 400-nm excitation the kinetics is dominated by 76 ps and 448 ps components, whereas a minor contribution stems from a 2-ns component (Fig. 1A). The latter time constant is not very accurately determined with the streak setup. The DAS of the 76 ps component peaks at ~690 nm, indicating that it contains a large contribution from PSI [8]. The two slowest components resolved from the streak-camera data (448 and 2 ns) are assigned to PSII according to their 680 nm peak [8]. The minor contribution with the relatively long lifetime of 2 ns probably originates from a small fraction of closed RCs and/or detached FCPs. In order to study the origin of the resolved components in more detail, additional streak-camera measurements were performed in the presence of 100 μM DCMU to close the PSII reaction centers (RCs) (Supplementary material), thereby increasing the corresponding PSII lifetimes, while the lifetimes of PSI are hardly affected [35,36]. The results show that in the presence of DCMU a very similar short component (76 ps) is observed (Fig. S3). Its lifetime, spectral shape and relative contribution are nearly identical to those observed for open RCs, demonstrating that this compartment is mainly due to PSI.

Global analysis of the streak-camera data obtained upon 535 nm excitation resolves three lifetimes: 134 ps, 681 ps and 2 ns. The components are characterized by rather complicated DAS shapes: both the 681-ps and 2-ns components have a peak at ~680 nm, indicating that they are mainly due to PSII. Moreover, a "red" shoulder around 700 nm–750 nm can also be observed in both cases. It is reminiscent of a broad plateau in the long-wavelength range, observed by Miloslavina et al. in case of NPQ measurements and it was assigned to a fluorescence antenna compartment, functionally disconnected from both PSI and PSII [8]. It was proposed that the FCPs that contribute to this red wing are in an aggregated state similar to oligomerized trimeric LHCII in higher plants [37]. The shortest component resolved by the streak setup in case of 535 nm excitation has a lifetime of 134 ps and a peak at 670 nm. Most importantly, upon 535-nm excitation, hardly any PSI spectral characteristics can be observed in the global analysis of the data, although the shoulder in the 690 nm region indicates that there is still some PSI contribution to the 134 ps component. However it is significantly smaller than in case of Chl *a* excitation, demonstrating that the FCPs that are preferentially excited at 535 nm transfer their excitation energy mainly to PSII. Additional measurements were done in the presence of DCMU which leads to the closure of PSII RCs and thus to longer fluorescence lifetimes. From the global analysis of the data measured on closed RCs we found that all resolved components had longer lifetimes than in the case of open PSII RCs (results not shown) in contrast to the measurements at 400 nm excitation where the PSI contribution remained unchanged (Fig. S3 in Supplementary material). Therefore it is concluded that the PSII contribution is dominating when the cells are excited at 535 nm excitation (Fig. 1B).

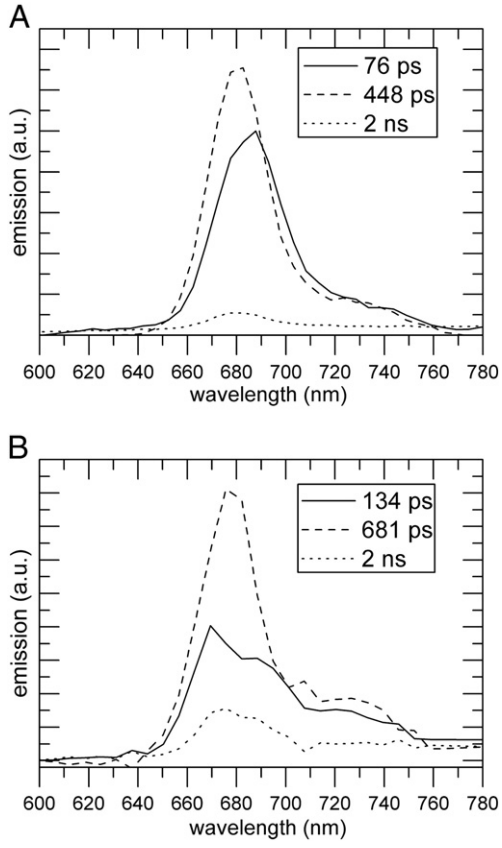

Fig. 1. DAS of *C. meneghiniana LL*, obtained after global analysis of streak-camera data. The corresponding lifetimes are given in the inset. Excitation wavelengths are 400 nm (A) and 535 nm (B). The time window is 2 ns.

In order to obtain better estimates of the fluorescence lifetimes for LL cells, the samples were also measured using the TCSPC technique. The excitation wavelength was either 400 nm or 535 nm and fluorescence was detected in the 671–724 nm region. The decay curves were fitted globally to a sum of exponential decay functions, except the longest component, that was left as a free parameter. In case of 400 nm excitation four components were needed to obtain a satisfactory fit for all wavelength combinations, as was judged from the Poissonian maximum likelihood estimator, and from the residuals and the autocorrelation function of the residuals. The lifetimes of the resolved components are 75 ps, 300 ps, 687 ps and 1.2–6 ns. For 535 nm excitation only three components are enough to get a satisfactory fit: 198 ps, 600 ps and 2.0–2.4 ns. The fitting results are summarized in Table 1.

The results obtained with the TCSPC setup upon 400 nm excitation are very similar to the streak-camera results. Again the shortest component (75 ps) has PSI characteristics with the amplitude peaking around 701 nm while the rest of the lifetimes should be assigned to open PSII (except for the 1.2–6 ns component that is due to closed RCs and/or detached FCPs). The main difference is the fact that the 448 ps component observed with the streak-camera setup is further resolved into a 300 ps and a 687 ps compartment in case of the TCSPC data. The average lifetime of these two components was calculated for each detection wavelength (Table 1, row τ_{PSII}) and turned out to be ~447 ps on average (τ_{PSII}, avg), which is virtually identical to the 448 ps lifetime as obtained from the streak-camera data and it is attributed to the average overall trapping time of excitations in PSII due to charge separation.

The average lifetime resolved from the TCSPC data in case of 535 nm excitation (~500 ps) is very close to the one obtained from the streak-camera measurements(~520 ps). But the resolved components in case of different techniques are somewhat different (198 ps, 600 ps for TCSPC vs. 134 ps and 681 ps for streak camera), while the amplitudes of the corresponding components are close to each other (the shortest component contributes ~60% while the second one ~35% of the 670–690 nm emission for both TCSPC and streak camera).

As can be judged from the average TCSPC lifetimes (τ_{avg}, τ'_{avg} Table 1), the fluorescence decay times after fx excitation are somewhat longer than for 400 nm excitation where Chl *a* is excited to a large extent. The contribution of the longest component is equally small in both cases, and it is not responsible for the observed difference (if it is excluded: τ'_{avg} (535 nm) − τ'_{avg} (400 nm) ≈ 140 ps; if included: τ_{avg} (535 nm) − τ_{avg} (400 nm) ≈ 150 ps, Table 1).

Like in the case of the streak-camera measurements the presence of a compartment mainly due to PSI is also not observed upon fx excitation in the TCSPC data, in agreement with the finding above that the FCP complexes that are excited at 535 nm, mainly transfer their excitation energy to PSII. The shortest component resolved by TCSPC is 198 ps

Table 1
C. meneghiniana LL results of global fitting of the TCSPC decay curves upon 400 nm and 535 nm excitation.

λ_{det} / τ	670 nm	679 nm	693 nm	701 nm	712 nm	724 nm	*avg
400 nm excitation							
75 ps	13%	19%	37%	44%	43%	41%	
300 ps	63%	53%	36%	30%	33%	31%	
687 ps	21%	26%	26%	24%	21%	26%	
1.2–6 ns	3%	2%	1%	2%	3%	2%	
$^{*}\tau_{avg}$, ps	391	372	330	325	326	328	345
$^{*}\tau'_{avg}$, ps	354	359	317	294	284	308	319
$^{*}\tau_{PSII}$, ps	397	427	462	472	450	476	447
535 nm excitation							
198 ps	32%	31%	34%	36%	38%	37%	35%
600 ps	67%	68%	63%	63%	61%	61%	64%
2.0–2.4 ns	1%	1%	3%	1%	1%	2%	1%
$^{*}\tau_{avg}$, ps	504	528	448	475	518	485	493
$^{*}\tau'_{avg}$, ps	470	469	459	454	446	462	460

The longest component was not fitted globally and was a free parameter in the analysis. Confidence intervals of fluorescence lifetimes were calculated by an exhaustive search algorithm and were <7% for the entire detection interval. Standard errors of amplitudes were estimated from 3 to 5 repetitions and were not higher than 5%.The 75 ps component is very similar to the 76 ps component obtained from the streak-camera data (400 nm excitation case). Its lifetime, spectral shape and relative contribution are all nearly identical to its counterpart for the streak measurements. It was demonstrated that this component is entirely due to PSI (Supplementary material), whereas the 300 ps and 687 ps compartments are assigned to the PSII kinetics in the TCSPC measurements upon 400 nm excitation.
avg, mean value of an amplitude/average lifetime over the whole detection region. In case of the amplitude, only the rows that do not show strong deviations throughout the detection region were averaged.
τ_{avg}, total average lifetime of the fluorescence decay.
τ'_{avg}, average lifetime of the fluorescence decays when the contribution of the longest component was omitted from the calculations. Its amplitude is very small and probably it originates from closed RCs of PSII or/and small fraction of detached FCPs, so for most of the estimations it is not of interest.
τ_{PSII}, overall charge separation time that was calculated as a weighted average lifetime of the 300 ps and 687 ps components.

with an amplitude of ~35% that shows only a few percent of variation for the different detection wavelengths.

To obtain further evidence that excitation energy is preferably transferred to PSII in case of selective antenna excitation at 535 nm, steady-state low-temperature spectra were recorded using 400 nm and 535 nm excitation at 77 K. Indeed Fig. 2 shows that the relative amount of PSI fluorescence is smaller upon 535 nm excitation.

From the two shortest components resolved by TCSPC at 535 nm the weighted average lifetime was determined at each detection wavelength and it is presented in the row τ'_{avg} of Table 1 (535 nm excitation part). Because both lifetimes are mainly due to PSII, τ'_{avg} can be considered as the overall average PSII trapping time ($\tau'_{avg} = \tau_{PSII}$). Its mean value for the whole detection region is 460 ps (τ'_{avg}, avg), which is ~13 ps longer than it was observed upon Chl *a* excitation (447 ps). The lengthening of the lifetime attributed to PSII is expected because the excitation at 535 nm leads to relatively more excitations in the antennas and thus to a longer migration time [38]. This finding is reminiscent of earlier data obtained for thylakoid membranes from *Arabidopsis thaliana*, where a difference in migration time led to a difference in the average lifetime of 13 ps after excitation at 484 and 412 nm [39]. Note that in that case the estimated migration time, i.e. the average time it takes for an excitation to reach the reaction center or primary electron donor for the first time, was around 150 ps.

3.2. PSI and PSII excitation spectra of C. meneghiniana

In order to obtain the PSI and PSII excitation spectra for intact *C. meneghiniana* cells use was made of the procedure described in Materials and methods. For obtaining the PSII excitation spectrum

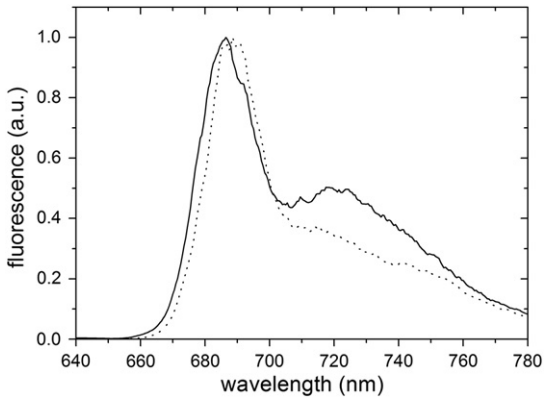

Fig. 2. Normalized 77 K Fluorescence emission spectra obtained upon 400 nm excitation (solid line) and 535 nm excitation (dotted line), indicating that 535-nm excitation leads to significantly less long-wavelength PSI fluorescence.

in vivo, steady-state measurements with and without DCMU were performed, while for obtaining the PSI excitation spectrum a scaling parameter was needed and it was calculated from the time-resolved measurements (Eqs. (5), (6)). Use was made of the time-resolved streak-camera data obtained with "open" RCs upon 400 nm excitation (Fig. 1A). It was shown above that the 76 ps component is mainly due to PSI while the 448 ps compartment can be considered as the overall trapping time of PSII. The contribution of PSII to the 76 ps DAS is very small, but the exact value is not known. Therefore, in order to estimate the PSI excitation spectrum we considered two rather extreme cases: 1) the 76 ps component is entirely due to PSI; 2) 20% of its amplitude is due to PSII (which is clearly an overestimation). The final shape of PSI excitation spectrum was very similar in both cases (data not shown). The origin of the longest component is not completely clear (most probably it originates from a small fraction of closed RCs or/and detached FCPs), and the scaling value was calculated by both including and excluding its contribution from the PSII estimations. This resulted only in a small variation of the $E_{PSI}^{ex/det}$ value (<4%), and the resulting PSI excitation spectra were nearly indistinguishable (data not shown). To verify these results the procedure was done for two detection wavelengths: 679 nm and 693 nm. From the DAS presented in Fig. 1A the following estimations of the PSI contribution to $Q^{ex/det}$ were obtained:

$$679\,\text{nm} \pm 5\,\text{nm}: E_{PSI}{}^{400/679} = 0.07;$$

$$693\,\text{nm} \pm 5\,\text{nm}: E_{PSI}{}^{400/693} = 0.11.$$

The extracted excitation spectra appeared to be independent of the detection wavelength, also confirming that the PSI and PSII kinetics were nicely separated in the time-resolved data. In Fig. 3 the obtained PSI and PSII excitation spectra are presented. As compared to the PSII spectrum, the PSI spectrum exhibits less contribution in the absorption region of the accessory antenna pigments (Chl *c* and fx) indicating again that FCPs transfer their excitation energy preferably to PSII.

Using the obtained spectra, we also tried to estimate whether the proportion of fx_{blue} and fx_{red} is different in case of FCPs bound to the different photosystems. There are some indications derived from *in vivo* measurements that fx_{red} is bound to PSII in a slightly higher amount than to PSI [9]. In order to compare the shape of the PSI and PSII excitation spectra, they were normalized at 500 nm and the spectral shoulders were compared in the fx absorption region (Fig. 3: insert). Both spectra appear to be very similar but the PSII excitation spectrum is red-shifted by 4 nm as compared to the PSI excitation spectrum. This is in qualitative agreement with results published

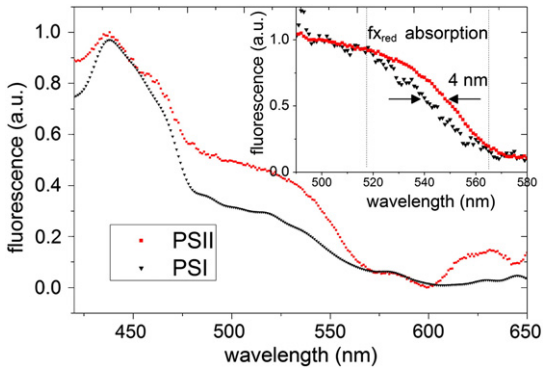

Fig. 3. Normalized fluorescence excitation spectra of PSI (black) and PSII (red) from *C. meneghiniana* LL cells extracted by the procedure described in the Materials and methods subsection. Insert: fluorescence excitation spectra normalized at 500 nm.

earlier by Szabo et al. [9], although the effect observed in the present study is less pronounced.

3.3. Fluorescence kinetics of LL-, ML- and HL-grown C. meneghiniana cells upon 535 nm excitation

C. meneghiniana cells grown in different light intensities (LL, ML, HL) were studied by time-resolved fluorescence using 535 nm and 400 nm excitation wavelengths. From the measurements reported in the previous section it was concluded that most of the excitation energy is transferred from FCPs to PSII RCs. In this subsection we monitor the difference in the fluorescence kinetics of *C. meneghiniana* cells grown in different light conditions (LL, ML, HL) after using the fx excitation wavelength (535 nm) in the TCSPC measurements. In Fig. 4, 679 nm TCSPC decay curves are presented of *C. meneghiniana* cells grown in different photon flux densities. Whereas there is no strong difference between the decay kinetics of the LL and ML samples, the decay curve of the HL cells is considerably faster. The global fitting results for the LL sample are given in Table 1. In case of ML and HL cultures, three decay components were needed to get satisfactory fits for all detection wavelengths (Table 2). The longest component (2.3–3.6 ns) was not fitted globally. Its contribution is very small (<3%) and it is assumed to be due to a small fraction of closed RCs or/and detached FCPs. Therefore, in Table 2 only τ'_{avg} is presented, which does not include the longest component. The value of τ'_{avg} for the HL culture is substantially smaller than for LL and ML cells. Although the lifetimes of the resolved components do not differ much for all three samples (165 and 619 ps for HL as compared to 189 ps and 641 ps for ML and 196 and 600 ps for LL), the relative contributions of the resolved components vary strongly: going from LL to HL the amplitude of the shortest component increases from ~35% to 56%, while the contribution of the second component decreases from 64% to 43%. Comparison of the fitting results of LL and ML samples shows that the ML average lifetimes are on average 35 ps shorter. The difference between HL and LL samples is even more striking: the LL average decay time is ~100 ps slower than that of the HL cells. As was stated before, the kinetics upon 535 nm excitation is dominated by PSII. That is why the calculated average lifetime upon fx excitation (τ'_{avg}) can be considered as the overall average trapping time of PSII ($\tau'_{avg} = \tau_{PSII}$). Then the 100 ps decrease of the τ_{PSII} value for the HL cells as compared to the LL cells reflects a difference in the antenna size.

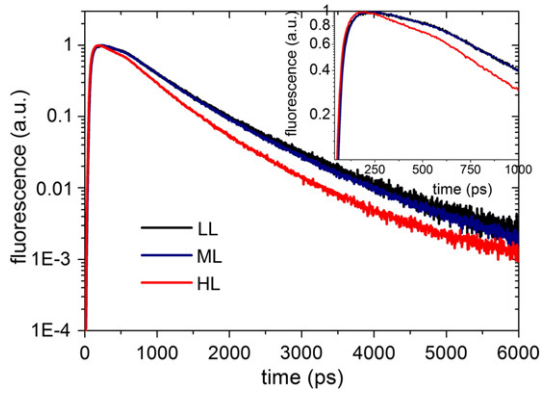

Fig. 4. TCSPC results for LL (black line), ML (blue line) and HL (red line) *C. meneghiniana* cells upon 535 nm excitation and 679 nm detection. Insert: initial part of the decay curves.

In higher plants it has been established that the LHCII/RC ratio strongly affects the overall average PSII decay lifetime. In case of PSII membranes (BBY preparations) from spinach [40] where this ratio was 2.35–2.55 a lifetime of ~150 ps was found by Broess et al. [41], while van Oort and coworkers observed an increase of the average PSII lifetime up to ~330 ps for thylakoid membranes with an LHCII/PSII ratio of 4.0 [39].

3.4. Fluorescence kinetics of LL-, ML- and HL- C. meneghiniana cells upon 400 nm excitation

In Fig. 5 a comparison is made between *C. meneghiniana* LL, ML, HL decay curves upon 400 nm excitation and 535 nm excitation. As was already explained above, 535 nm excitation leads to a longer average PSII trapping time for LL cells than for HL cells upon fx excitation, due to the difference in antenna size.

However, for ML and HL cells the fluorescence kinetics upon 400 nm excitation are considerably slower than upon 535 nm excitation, meaning that apart from a reduction in the antenna size, also some other changes take place upon increasing the light intensity during growth. The global analysis of TCSPC ML and HL data is presented in Table 3. The value of τ_{avg} increases by ~100 ps for ML cells as compared to LL cells (~391 ps for LL, ~488 ps for ML). This difference is remarkable because the growth irradiance for ML is only 30 μmol photons m^{-2} s^{-1} higher than in case of the culture grown in low light. For HL cells the average lifetime increases even further up to ~520 ps. From the global analysis of the ML data (Table 3) the PSI component is found to be 68 ps. Its amplitude varies a lot and peaks at 701 nm. This result is similar as for LL cells where a PSI

Table 2
Results of global fitting of the fluorescence decay curves of *C. meneghiniana* upon 535 nm excitation.

λ det	670 nm	679 nm	693 nm	701 nm	712 nm	724 nm	*avg
τ							
C. meneghiniana ML							
189 ps	51%	47%	45%	45%	46%	46%	47%
641 ps	47%	52%	52%	54%	51%	51%	51%
2.3–3.6 ns	2%	1%	3%	1%	3%	3%	2%
$^*\tau'_{avg}$, ps	406	426	431	436	426	426	425
C. meneghiniana HL							
165 ps	58%	56%	53%	55%	60%	53%	56%
619 ps	41%	43%	45%	44%	40%	45%	43%
2.7–3.6 ns	1%	1%	2%	1%	<1%	2%	1%
$^*\tau'_{avg}$, ps	353	364	373	367	347	373	363

The longest component was not fitted globally and was a free parameter in the analysis. Confidence intervals of fluorescence lifetimes were calculated by exhaustive search algorithm and were <4% through all detection interval. Standard errors of amplitudes were calculated from 3-5 repeats and were not more than 3%.
avg, mean value of an amplitude/average lifetime over the whole detection region.
τ'_{avg}, average lifetime of the fluorescence decays when the contribution of the longest component was omitted from the calculations. Its amplitude is very small and probably it originates from closed RCs of PSII or/and small fraction of detached FCPs.

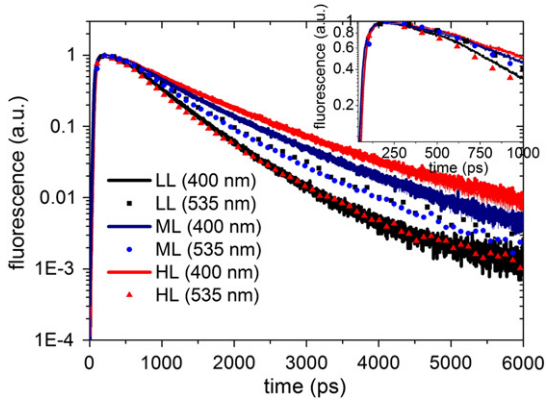

Fig. 5. Time-resolved (TCSPC) fluorescence kinetics of *C. meneghiniana* LL (black), ML(blue) and HL (red) cells detected at 679 nm using 400 nm (lines) and 535 nm excitation (dots). Insert: initial part of the decay curves.

75 ps component was observed (Table 1). The main difference between the LL and ML results stems from the longest component (LL: 1.2–6 ns; ML: 1.5–1.9 ns) which has a far higher amplitude for ML cells, even up to 8%, which is almost 3 times higher as was observed for LL cells. It can neither be assigned to detached FCPs nor to closed RCs attached to FCPs because the component does not have a counterpart upon 535 nm excitation (Table 2). Therefore, it most probably originates either from non-functioning PSII (inactivated/disassembled PSII units) or PSII with closed RCs that are disconnected from the antenna complexes.

HL results show that the kinetics of PSI cannot be completely resolved anymore from the TCSPC data. The shortest component that was resolved for the HL cells upon 400 nm excitation is 122 ps. Its amplitude contribution varies between 49 and 54% over the entire detection window without showing any specific peaks. This provides direct evidence for a significant decrease of functional PSI for cultures grown in high-light intensities. This result is in agreement with the results of Strzepek and Harrison, who detected a strong decrease of the PSI concentration with an increase of the growth irradiance for the diatom *Thalassiosira weissflogii* [20]. It is also in line with Beer et al, who measured a slower PSII reoxidation in HL cells of *C. meneghiniana* [42].The second component resolved in HL is 803 ps with a contribution of ~41% throughout the whole detection region, and this lifetime is somewhat longer than in case of LL, ML samples, where 687 ps (LL) and 764 ps (ML) lifetimes were obtained.

Another aspect that contributes to the increase of the average lifetime is similar as for the ML culture: a strong increase of the amplitude of the slowest component (1.7–2.4 ns) up to 8%. Again, this rise is not observed upon 535 nm excitation.

So upon relatively selective Chl *a* excitation a strong increase of the average fluorescence lifetime was observed for ML and HL cultures which is due to two main effects: a decrease in the relative amount of PSI and an increase of Chl *a* that is not active in excitation energy transfer and most probably attached to inactivated/disassembled PSII units as a result of photoinhibition [43]. This hypothesis is in agreement with the observation that the maximum quantum yield of PSII photochemistry (F_v/F_m) decreases substantially under HL growing conditions as compared to LL[42],[20]. Interestingly this effect is already substantial for the ML culture, where the growth irradiance was (only) 50 μmol photons m^{-2} s^{-1}.

Table 3
Global fitting results of the *C. meneghiniana* (ML and HL) decay curves upon 400 nm excitation.

λ_{det} / τ	670 nm	679 nm	693 nm	701 nm	712 nm	724 nm	*avg
C. meneghiniana ML							
68 ps	8%	23%	36%	48%	46%	47%	
241 ps	43%	25%	22%	13%	14%	12%	
764 ps	46%	45%	38%	33%	32%	33%	
1.5–1.9 ns	3%	7%	4%	6%	8%	7%	
τ_{avg}, ps	500	516	480	470	470	493	488
C. meneghiniana HL							
122 ps	53%	55%	50%	54%	54%	49%	53%
803 ps	40%	40%	44%	40%	40%	42%	41%
1.7–2.4 ns	7%	5%	6%	6%	~6%	~8%	6%
τ_{avg}, ps	507	544	517	516	529	527	523

The longest component was not fitted globally and was left as a free parameter in the analysis. Confidence intervals of fluorescence lifetimes were calculated by exhaustive search algorithm and were <6% through all detection interval. Standard errors of amplitudes were calculated from 3 to 5 repeats and were not larger than 3%.
avg, mean value of an amplitude/average lifetime over the whole detection region. In case of the amplitude, only the rows that do not show strong deviations throughout the detection region were averaged.

4. Discussion

In this work we have investigated and interpreted the variation in fluorescence kinetics of the diatom *C. meneghiniana in vivo* grown in different light conditions. Use was made of different excitation wavelengths to preferentially excite antenna or core complexes and different detection wavelengths were used to discriminate between PSI and PSII. The combination of steady-state and time-resolved fluorescence allowed us to distinguish between the excitation spectra of PSI and PSII.

400 nm excitation of low-light cultures leads to a 75 ps lifetime that mainly corresponds to excitation trapping in PSI, which is close to the lifetime of PSI in higher plants [27,44,45]. For PSII an average lifetime of 448 ps is found. These results are reminiscent of those obtained for thylakoid membranes from *Arabidopsis thaliana* [39], where the average fluorescence lifetime of PSII was reported to be ~333 ps and a 73 ps lifetime was found that was predominantly due to PSI. The longer lifetime for PSII in *C. meneghiniana* LL cells may be due to a larger antenna size (the *Arabidopsis* thylakoids contained ~300 pigments/RC [39,46,47]) although it should be realized that the antenna composition differs and the same is true for its organization. A larger antenna size allows more effective light harvesting in LL growing conditions as shown by Smith and Melis in diatoms [22], while high photon flux densities cause a decrease of the antenna size that is also reflected in the average lifetimes (see below). It is worth mentioning that the DAS for our PSI and PSII components are very similar in shape as those reported by Miloslavina et al. with the same peak positions (~680 nm for PSII and ~690 nm for PSI) [8]. In that study three components for both PSI and PSII were observed by performing target model fitting (*C. meneghiniana*: 2.6 ps, 12 ps, 66 ps for PSI and 159 ps, 300 ps and 580 ps for PSII). A rough average lifetime estimation for their results leads to ~51 ps for PSI and ~395 ps for PSII (*C. meneghiniana*). These values are slightly shorter than in our case but, as was shown above, the growth conditions can influence the average lifetimes. We conclude that the antenna size for the samples used by Miloslavina et al. were smaller, probably as a result of different illumination conditions used during growth (reported intensity was 40 μmol photons m^{-2} s^{-1}).

In case of selective antenna excitation at 535 nm we observed that PSI was excited rather poorly and no PSI can be distinguished by the global analysis of the data. Furthermore the PSII-associated antenna seems to be enriched in fx_{red} (Fig. 3: Insert), indicating that the FCPb oligomeric form can be not only connected to PSI [19] but also to PSII.

The decrease of the PSI contribution upon fx excitation at 535 nm results in the fact that the kinetics starts to be dominated by two components, both of which are predominantly attributed to PSII and the lifetimes are around 460 ps on average (Table 1, τ'_{avg}). This

value is ~13 ps longer than the average PSII lifetime observed upon Chl *a* excitation (449 ps), due to an increase of the migration time when there are relatively more excitations in the outer antenna. We cannot estimate the difference in migration time very accurately because it is not possible yet to completely correct for the PSI kinetics both at 400 nm and at 535 nm and moreover the ratio of PSII core and antenna excitations at 400 nm is not known.

We have observed a strong effect of growth light conditions on the PSII fluorescence kinetics. In case of selective antenna excitation, the average lifetime decreased from 460 ps for LL- to 363 ps in case of HL-cultures. The ~100 ps shortening reflects a decrease of the FCP antenna size connected to the RC of PSII. In this respect our results agree with those of Gallagher et al. [23]. On the other hand our findings are in disagreement with those of Lepetit and co-workers, who claimed that the number of antenna complexes per RC is relatively constant in different light regimes [25].

In case of higher plants, it was shown that the size of the PSII antenna influences the fluorescence lifetimes substantially [46,48]. For membranes that contain 2.0–2.5 LHCII trimers per PSII RC, the fluorescence lifetime was reported to be around 150 ps upon Chl *a* excitation [38,41] whereas for thylakoid membranes with 4.0 trimers per PSII RC, the lifetime goes up to around 330 ps [39,46,48], partly because the extra trimers are connected less well with the RC. Although significant sequence similarity exists between FCP and LHCII proteins the antenna composition and organization differs. In diatoms, special FCP proteins (Lhcr) are bound to PSI only [19,49,50], whereas no data about the precise organization of the PSII antenna composition exists. Both FCPa and FCPb complexes were isolated separately from the photosystems and consist of Lhcf proteins, whereby FCPa contain Lhcx polypeptides in addition [5]. As mentioned above, only hints exist about the attribution of FCP complexes to either photosystem. The enrichment of the PSII antenna with fx_{red} points at least to FCPb being associated with PSII. Thus we tentatively assume that losing one FCPb from the PSII antenna might be responsible for the difference in PSII lifetime for LL and HL cells. Such a change in PSU size would not result in a detectable change in the relative pigment concentrations, making these values less good indicators for the antenna size change in contrast to what was assumed in [25].

The results obtained for the light-treated cells upon 400-nm excitation demonstrate that apart from the PSII antenna size also other changes occur. Increasing the growth irradiance leads to a relative decrease of the amount of PSI as compared to PSII, which is reflected by the fact that the ~70 ps PSI lifetime cannot be resolved anymore in case of HL cells. Moreover, the samples grown in ML- and HL-conditions start to experience strong photoinhibition. This effect manifests itself by a substantial increase of the contribution of long lifetime components. This is reminiscent of results obtained by Wu et al. [43], who observed large pools of inactive or disassembled PSII centers in *Thalassiosira pseudonana* in case of a sudden increase of irradiance.

Acknowledgements

The authors thank Rob Koehorst and Arie van Hoek for technical help with the measurements, Cor Wolfs for initial help with growing cells and Sergey Laptenok, Joris Snellenburg and Ivo van Stokkum for seminal support in the usage of the Glotaran software analysis toolkit. This work was supported by HARVEST Marie Curie Research Training Network (PITN-GA-2009-238017) to VUC.

Appendix A. Supplementary data

Details about the experimental conditions and comparison of streak-camera DAS obtained from *C. meneghiniana* LL in "open" state and in the presence of DCMU upon 400 nm excitation can be found in the Supplementary material. Supplementary data associated with this article can be found, in the online version, at http://dx.doi.org/10.1016/j.bbabio.2012.09.015.

References

[1] P.G. Falkowski, R.T. Barber, V. Smetacek, Biogeochemical controls and feedbacks on ocean primary production, Science 281 (1998) 200–206.
[2] C. Wilhelm, C. Büchel, J. Fisahn, R. Goss, T. Jakob, J. Laroche, J. Lavaud, M. Lohr, U. Riebesell, K. Stehfest, K. Valentin, P.G. Kroth, The regulation of carbon and nutrient assimilation in diatoms is significantly different from green algae, Protist 157 (2006) 91–124.
[3] J. Lavaud, Fast regulation of photosynthesis in diatoms: mechanisms, evolution and ecophysiology, Func. Plant Sci. Biotech. 1 (2007) 267–287.
[4] E. Papagiannakis, I.H.M. van Stokkum, H. Fey, C. Büchel, R. van Grondelle, Spectroscopic characterization of the excitation energy transfer in the fucoxanthin-chlorophyll protein of diatoms, Photosynth. Res. 86 (2005) 241–250.
[5] A. Beer, K. Gundermann, J. Beckmann, C. Büchel, Subunit composition and pigmentation of fucoxanthin-chlorophyll proteins in diatoms: evidence for a subunit involved in diadinoxanthin and diatoxanthin binding, Biochemistry 45 (2006) 13046–13053.
[6] N. Gildenhoff, S. Amarie, K. Gundermann, A. Beer, C. Büchel, J. Wachtveitl, Oligomerization and pigmentation dependent excitation energy transfer in fucoxanthin-chlorophyll proteins, Biochim. Biophys. Acta 1797 (2010) 543–549.
[7] L. Premvardhan, B. Robert, A. Beer, C. Büchel, Pigment organization in fucoxanthin chlorophyll a/c(2) proteins (FCP) based on resonance Raman spectroscopy and sequence analysis, Biochim. Biophys. Acta Bioenerg. 1797 (2010) 1647–1656.
[8] Y. Miloslavina, I. Grouneva, P.H. Lambrev, B. Lepetit, R. Goss, C. Wilhelm, A.R. Holzwarth, Ultrafast fluorescence study on the location and mechanism of non-photochemical quenching in diatoms, Biochim. Biophys. Acta 1787 (2009) 1189–1197.
[9] M. Szabo, L. Premvardhan, B. Lepetit, R. Goss, C. Wilhelm, G. Garab, Functional heterogeneity of the fucoxanthins and fucoxanthin-chlorophyll proteins in diatom cells revealed by their electrochromic response and fluorescence and linear dichroism spectra, Chem. Phys. 373 (2010) 110–114.
[10] W.W. Su, T. Jakob, C. Wilhelm, The impact of nonphotochemical quenching of fluorescence on the photon balance in diatoms under dynamic light conditions, J. Phycol. 48 (2012) 336–346.
[11] D.G. Durnford, R. Aebersold, B.R. Green, The fucoxanthin-chlorophyll proteins from a chromophyte alga are part of a large multigene family: structural and evolutionary relationships to other light harvesting antennae, Mol. Gen. Genet. 253 (1996) 377–386.
[12] Z. Liu, H. Yan, K. Wang, T. Kuang, J. Zhang, L. Gui, X. An, W. Chang, Crystal structure of spinach major light-harvesting complex at 2.72 A resolution, Nature 428 (2004) 287–292.
[13] C. Büchel, Fucoxanthin-chlorophyll proteins in diatoms: 18 and 19 kDa subunits assemble into different oligomeric states, Biochemistry 42 (2003) 13027–13034.
[14] L. Premvardhan, L. Bordes, A. Beer, C. Büchel, B. Robert, Carotenoid structures and environments in trimeric and oligomeric fucoxanthin chlorophyll a/c(2) proteins from resonance Raman spectroscopy, J. Phys. Chem. B 113 (2009) 12565–12574.
[15] L. Premvardhan, D.J. Sandberg, H. Fey, R.R. Birge, C. Büchel, R. van Grondelle, The charge-transfer properties of the S-2 state of fucoxanthin in solution and in fucoxanthin chlorophyll-a/c(2) protein (FCP) based on stark spectroscopy and molecular-orbital theory, J. Phys. Chem. B 112 (2008) 11838–11853.
[16] T. Brakemann, W. Schlormann, J. Marquardt, M. Nolte, E. Rhiel, Association of fucoxanthin chlorophyll a/c-binding polypeptides with photosystems and phosphorylation in the centric diatom *Cyclotella cryptica*, Protist 157 (2006) 463–475.
[17] Y. Ikeda, M. Komura, M. Watanabe, C. Minami, H. Koike, S. Itoh, Y. Kashino, K. Satoh, Photosystem I complexes associated with fucoxanthin-chlorophyll-binding proteins from a marine centric diatom, *Chaetoceros gracilis*, Biochim. Biophys. Acta 1777 (2008) 351–361.
[18] R. Nagao, A. Ishii, O. Tada, T. Suzuki, N. Dohmae, A. Okumura, M. Iwai, T. Takahashi, Y. Kashino, I. Enami, Isolation and characterization of oxygen-evolving thylakoid membranes and Photosystem II particles from a marine diatom *Chaetoceros gracilis*, Biochim. Biophys. Acta 1767 (2007) 1353–1362.
[19] T. Veith, J. Brauns, W. Weisheit, M. Mittag, C. Büchel, Identification of a specific fucoxanthin-chlorophyll protein in the light harvesting complex of Photosystem I in the diatom *Cyclotella meneghiniana*, Biochim. Biophys. Acta Bioenerg. 1787 (2009) 905–912.
[20] R.F. Strzepek, P.J. Harrison, Photosynthetic architecture differs in coastal and oceanic diatoms, Nature 431 (2004) 689–692.
[21] P.G. Falkowski, T.G. Owens, A.C. Ley, D.C. Mauzerall, Effects of growth irradiance levels on the ratio of reaction centers in two species of marine phytoplankton, Plant Physiol. 68 (1981) 969–973.
[22] B.M. Smith, A. Melis, Photochemical apparatus organization in the diatom *Cylindrotheca fusiformis*: photosystem stoichiometry and excitation distribution in cells grown under high and low irradiance, Oxford University Press, Oxford, ROYAUME-UNI, 1988.
[23] J.C. Gallagher, A.M. Wood, R.S. Alberte, Ecotypic differentiation in the marine diatom skeletonema-costatum — influence of light-intensity on the photosynthetic apparatus, Mar. Biol. 82 (1984) 121–134.
[24] L. Provasoli, J.J.A. Mclaughlin, M.R. Droop, The development of artificial media for marine algae, Arch. Microbiol. 25 (1957) 392–428.
[25] B. Lepetit, D. Volke, M. Gilbert, C. Wilhelm, R. Goss, Evidence for the existence of one antenna-associated, lipid-dissolved and two protein-bound pools of diadinoxanthin cycle pigments in diatoms, Plant Physiol. 154 (2010) 1905–1920.

[26] O.J. Somsen, L.B. Keukens, M.N. de Keijzer, A. van Hoek, H. van Amerongen, Structural heterogeneity in DNA: temperature dependence of 2-aminopurine fluorescence in dinucleotides, Chemphyschem 6 (2005) 1622–1627.
[27] B. van Oort, A. Amunts, J.W. Borst, A. van Hoek, N. Nelson, H. van Amerongen, R. Croce, Picosecond fluorescence of intact and dissolved PSI-LHCI crystals, Biophys. J. 95 (2008) 5851–5861.
[28] A.V. Digris, V.V. Skakoun, E.G. Novikov, A. van Hoek, A. Claiborne, A.J.W.G. Visser, Thermal stability of a flavoprotein assessed from associative analysis of polarized time-resolved fluorescence spectroscopy, Eur. Biophys. J. Biophy. 28 (1999) 526–531.
[29] E.G. Novikov, A. van Hoek, A.J.W.G. Visser, J.W. Hofstraat, Linear algorithms for stretched exponential decay analysis, Opt. Commun. 166 (1999) 189–198.
[30] B. van Oort, S. Murali, E. Wientjes, R.B.M. Koehorst, R.B. Spruijt, A. van Hoek, R. Croce, H. van Amerongen, Ultrafast resonance energy transfer from a site-specifically attached fluorescent chromophore reveals the folding of the N-terminal domain of CP29, Chem. Phys. 357 (2009) 113–119.
[31] I.H. van Stokkum, B. van Oort, F. van Mourik, B. Gobets, H. van Amerongen, (Sub)-Picosecond Spectral Evolution of Fluorescence Studied with a Synchroscan Streak-Camera System and Target Analysis, in: Biophysical Techniques in Photosynthesis, Springer, Dordrecht, 2008, pp. 223–240.
[32] K.M. Mullen, I.H.M. van Stokkum, TIMP: An R package for modeling multi-way spectroscopic measurements, J. Stat. Softw. 18 (2007).
[33] J.J. Snellenburg, S. Laptenok, R. Seger, K.M. Mullen, I.H.M. van Stokkum, Glotaran: a Java-based graphical user interface for the R-package TIMP, J. Stat. Softw. 49 (2012) 1–23.
[34] I.H.M. van Stokkum, B. Gobets, T. Gensch, F. van Mourik, K.J. Hellingwerf, R. van Grondelle, J.T.M. Kennis, (Sub)-picosecond spectral evolution of fluorescence in photoactive proteins studied with a synchroscan streak camera system, Photochem. Photobiol. 82 (2006) 380–388.
[35] E. Wientjes, R. Croce, PMS: Photosystem I electron donor or fluorescence quencher, Photosynth. Res. 111 (2012) 185–191.
[36] M. Byrdin, I. Rimke, E. Schlodder, D. Stehlik, T.A. Roelofs, Decay kinetics and quantum yields of fluorescence in Photosystem I from *Synechococcus elongatus* with P700 in the reduced and oxidized state: are the kinetics of excited state decay trap-limited or transfer-limited? Biophys. J. 79 (2000) 992–1007.
[37] Y. Miloslavina, A. Wehner, P.H. Lambrev, E. Wientjes, M. Reus, G. Garab, R. Croce, A.R. Holzwarth, Far-red fluorescence: a direct spectroscopic marker for LHCII oligomer formation in non-photochemical quenching, FEBS Lett. 582 (2008) 3625–3631.
[38] K. Broess, G. Trinkunas, A. van Hoek, R. Croce, H. van Amerongen, Determination of the excitation migration time in Photosystem II consequences for the membrane organization and charge separation parameters, Biochim. Biophys. Acta 1777 (2008) 404–409.
[39] B. van Oort, M. Alberts, S. de Bianchi, L. Dall'Osto, R. Bassi, G. Trinkunas, R. Croce, H. van Amerongen, Effect of antenna-depletion in Photosystem II on excitation energy transfer in *Arabidopsis thaliana*, Biophys. J. 98 (2010) 922–931.
[40] D.A. Berthold, G.T. Babcock, C.F. Yocum, A highly resolved, oxygen-evolving photosystem-II preparation from spinach thylakoid membranes — electron-paramagnetic-Res and electron-transport properties, FEBS Lett. 134 (1981) 231–234.
[41] K. Broess, G. Trinkunas, C.D. van der Weij-de Wit, J.P. Dekker, A. van Hoek, H. van Amerongen, Excitation energy transfer and charge separation in Photosystem II membranes revisited, Biophys. J. 91 (2006) 3776–3786.
[42] A. Beer, M. Juhas, C. Büchel, Influence of different light intensities and different iron nutrition on the photosynthetic apparatus in the diatom *Cyclotella meneghiniana* (Bacillariophyceae), J. Phycol. 47 (2011) 1266–1273.
[43] H. Wu, A.M. Cockshutt, A. McCarthy, D.A. Campbell, Distinctive Photosystem II photoinactivation and protein dynamics in marine diatoms, Plant Physiol. 156 (2011) 2184–2195.
[44] E. Wientjes, G.T. Oostergetel, S. Jansson, E.J. Boekema, R. Croce, The role of Lhca complexes in the supramolecular organization of higher plant Photosystem I, J. Biol. Chem. 284 (2009) 7803–7810.
[45] E. Wientjes, I.H. van Stokkum, H. van Amerongen, R. Croce, The role of the individual Lhcas in Photosystem I excitation energy trapping, Biophys. J. 101 (2011) 745–754.
[46] R. Croce, H. van Amerongen, Light-harvesting and structural organization of Photosystem II: from individual complexes to thylakoid membrane, J. Photochem. Photobiol. B 104 (2011) 142–153.
[47] D. Sandonà, R. Croce, A. Pagano, M. Crimi, R. Bassi, Higher plants light harvesting proteins. Structure and function as revealed by mutation analysis of either protein or chromophore moieties, Biochim. Biophys. Acta Bioenerg. 1365 (1998) 207–214.
[48] S. Caffarri, K. Broess, R. Croce, H. van Amerongen, Excitation energy transfer and trapping in higher plant Photosystem II complexes with different antenna sizes, Biophys. J. 100 (2011) 2094–2103.
[49] T. Veith, C. Büchel, The monomeric Photosystem I-complex of the diatom *Phaeodactylum tricornutum* binds specific fucoxanthin chlorophyll proteins (FCPs) as light-harvesting complexes, Photosynth. Res. 91 (2007) 164–165.
[50] I. Grouneva, A. Rokka, E.M. Aro, The thylakoid membrane proteome of two marine diatoms outlines both diatom-specific and species-specific features of the photosynthetic machinery, J. Proteome Res. 10 (2011) 5338–5353.